PPPL-3237 - Preprint: February 1997, UC-426

Local Transport Barrier Formation and Relaxation in Reverse-Shear Plasmas on the TFTR Tokamak

E.J. Synakowski, S.H. Batha,[a] M.A. Beer, M.G. Bell, R.E. Bell, R.V. Budny, C.E. Bush,[b] P.C. Efthimion, T.S. Hahm, G.W. Hammett, B. LeBlanc, F. Levinton,[a] E. Mazzucato, H. Park, A.T. Ramsey, G. Schmidt, G. Rewoldt, S.D. Scott, G. Taylor, M.C. Zarnstorff

Princeton Plasma Physics Laboratory, Princeton University, Princeton, NJ 08543

Abstract: The roles of turbulence stabilization by sheared E×B flow and *Shafranov*-shift gradients are examined for TFTR [Plasma Phys. Controlled Nucl. Fusion Res. **26**, 11 (1984)] Enhanced Reverse-Shear plasmas. Both effects in combination provide the basis of a positive-feedback model that predicts reinforced turbulence suppression with increasing pressure gradient. Local fluctuation behavior at the onset of ERS confinement is consistent with this framework. The power required for transitions into the ERS regime are lower when high power neutral beams are applied earlier in the current profile evolution, consistent with the suggestion that both effects play a role. Separation of the roles of E×B and Shafranov shift effects was performed by varying the E×B shear through changes in the toroidal velocity with nearly-steady-state pressure profiles. Transport and fluctuation levels increase only when E×B shearing rates are driven below a critical value that is comparable to the fastest linear growth rates of the dominant instabilities. While a turbulence suppression criterion that involves the ratio of shearing to linear growth rates is in accord with many of these results, the existence of hidden dependencies of the criterion is suggested in experiments where the toroidal field was varied. The forward transition into the ERS regime has also been examined in strongly rotating plasmas. The power threshold is higher with unidirectional injection than with balanced injection.

PACS numbers: 52.55.Fa, 52.25.Fi, 52.55.Dy, 52.35.Ra

(a) Fusion Physics and Technology, Torrance, California 90503.
(b) Oak Ridge National Laboratory, Oak Ridge, Tennessee 37830.

I. Introduction

The physics of confinement bifurcations in the edge of tokamak plasmas has been the topic of experimental and theoretical studies for many years. More recently, attention has focused on confinement bifurcations in the plasma core. Enhanced Reversed Shear (ERS)[1] plasmas obtained in the Tokamak Fusion Test Reactor [Plasma Phys. Controlled Nucl. Fusion Res. **26**, 11 (1984)] and DIII-D Negative Central Shear (NCS)[2] plasmas possess transport barriers deep in the core. The central regions in these plasmas are characterized by low energy, particle, and momentum transport. These confinement characteristics yield large pressure gradients and velocity shears, which lead to the inference that these plasmas possess large radial electric fields E_r, and large electric field gradients. While it has been pointed out[3,4] that these strong shears are correlated with the good confinement, it remains an open question whether E_r and E×B flow shear[5,6] plays a causative role in reducing transport in these cases, much as the dominant working hypothesis for edge plasma transport bifurcations suggests.[7,8,9,10] While E_r plays a central role in proposed mechanisms for ERS transitions on TFTR,[11] other proposals have been made in which it is not required. One such alternative[12,13,14] is based on the role of the large Shafranov shifts Δ these plasmas possess as a result of low core current densities and high neutral beam heating powers. These shifts are expected to suppress the turbulence by inducing a favorable drift precession of barely trapped electrons, thus reducing the drive for the dominant instabilities. In both of the above scenarios, good confinement is expected to be reinforced by the stabilization of ion-thermal-gradient turbulence from the peaking of the density profile.[15]

This work examines the possibility that one or both of these effects plays a role in ERS plasma development and sustainment. In Section II, an overview of the plasma parameters is provided. In Section III, the means of inferring E_r is described. Turbulence shearing rates are introduced, and some background comments about the linear growth rate calculations are made. Section IV contains several points. First is a description of the bifurcating nature of TFTR reverse-shear plasmas. Second is a discussion of the possible roles of both E×B shear flow and large Shafranov shift gradient. The expected threshold character of ExB shear suppression[5] is discussed.

A transition model based on both effects is outlined, and its characteristics are compared to core fluctuation data. The application of high power injection at different times in the current profile evolution, and the resultant scaling of the ERS power threshold, are discussed in Section V. This scaling is examined in the context of both E×B and Shafranov shift gradient turbulence suppression scenarios. Section VI outlines results from experiments designed to separate the roles of E×B shear and Shafranov shift gradient. This was performed by varying the applied torque in ERS plasmas of nearly constant plasma pressure. In Section VII, the shear suppression criterion of Ref. 5 is examined. The implications of ERS threshold experiments performed by varying the toroidal field at constant q, as well as the plasma rotation, are highlighted. Section VII contains a summary of results and a discussion of some implications.

II. General plasma description

In all of the experiments described here, reverse magnetic shear (RS) plasmas were generated in the standard way[1] by heating them with modest neutral beam power (7 MW) during the period of current ramp-up. Transitions to the ERS regime are obtained with a period of 350 - 500 ms of high-power beam heating (15-30 MW), depending on toroidal magnetic field and plasma current. During this period the central electron density increases rapidly due to strong core particle fueling and improved core particle confinement, reaching 7 - 12×10^{19} m^{-3}, depending on injection power and duration. At the highest powers, the injection is in a balanced configuration having nearly equal power injected tangentially parallel (co) and antiparallel (counter) to the plasma current. Deviations from this balanced injection scheme give a means of varying the plasma rotation and thus the radial electric field, as discussed later in this work. All of the plasmas examined here had a toroidal field B_T of 4.6 T and a plasma current of 1.6 MA, except in the case of the B_T scaling experiment (Section VII). Plasmas discussed in Sections V and VI also had a lithium pellet injected 500 ms before the onset of high power beams. Although lithium pumps out of the target plasma on this time scale, its injection has the beneficial effect of lowering the power threshold for ERS transitions. This is being examined in light of the proposed threshold mechanisms presented in this paper. These pellets have only a small effect on the measured q profile at the time of high powered injection.

III. E×B flow shear determination, linear growth rate calculations, and a shear suppression criterion

In what follows, reference is made to the shearing rates $\gamma_{E\times B}$ and the linear growth rate of the fastest growing mode γ_{lin}^{max} , maximized over all wave numbers k. The growth rates were calculated with a gyrofluid treatment[16] that includes the role of Δ', but excludes the effects of E×B shear. In these plasmas, modes are expected to become unstable primarily by the trapped electron precession resonance, and are generally classified as trapped electron modes (TEM).

In a toroidal geometry, the gradient in the quantity E_r/RB_θ characterizes the shearing of turbulence, where R is the major radius.[6] In a tokamak plasma of arbitrary shape, a characteristic rate for shearing turbulence can be written as

$$\gamma_{E\times B} = \frac{\Delta\Psi_0}{\Delta\phi}\left[\frac{\partial}{\partial\Psi}\left(\frac{E_r}{RB_\theta}\right)\right] \qquad (1)$$

where Ψ is the poloidal magnetic flux, $\Delta r_0 \equiv \Delta\Psi_0/RB_\theta$ is the radial correlation length, and $\Delta\phi$ is the toroidal correlation angle. Assuming isotropy of turbulence in the plane perpendicular to the magnetic field, which is roughly supported by nonlinear simulations,[5,15] leads to a simpler expression valid on the outer midplane,[17]

$$\gamma_{E\times B} = E_r/B\,[\,1/E_r(\partial E_r/\partial R) - 1/B_\theta(\partial B_\theta/\partial R) - 1/R] \qquad (2)$$

where B is the total magnetic field magnitude. Since it is assumed that the underlying turbulence has a ballooning character, the outer midplane is regarded as the region where E×B shear has to be effective in order to suppress turbulence. Such ballooning character has been observed in reflectometry measurements on TFTR. Note that any direct role of shear reversal in determining the shearing rate comes through the scale length of B_θ, and not B_θ itself.

For any plasma species, the radial force balance equation is given by

$$E_r = \nabla p/(nZe) + V_\phi B_\theta - V_\theta B_\phi \qquad (3)$$

where n is the density of the species in question, p is the pressure, Z is the charge number, e is the electronic charge, V_θ is the poloidal rotation, V_ϕ is the toroidal rotation, B_θ is the poloidal magnetic field, and B_ϕ is the toroidal field. In determining E_r, B_θ was measured with the Motional Stark Effect diagnostic[18] when contributions from the plasma E_r to the total electric field experienced by the beam neutrals were small.[19] During high power injection, TRANSP calculations were used to obtain B_θ. The accuracy of this procedure and its influence on the shearing rate was tested by comparing measured and calculated values of $1/B_\theta \partial B_\theta/\partial R$ for plasmas with reduced beam power, resulting in the plasma's E_r being much smaller than the total field experienced in a beam neutral's frame. Starting with a measured profile of B_θ, TRANSP projections of $1/B_\theta \partial B_\theta/\partial R$ agree with measured values to within 10% over time intervals corresponding to those of interest in the plasmas discussed here. The carbon toroidal velocity V_ϕ and the carbon pressure p_c were measured with charge exchange recombination spectroscopy,[20] and V_θ was calculated with the NCLASS code using the neoclassical treatment of Hirshman and Sigmar.[21] Regarding the calculation of V_θ, measurements of differences in E_r in supershot plasma conditions with similar pressure profiles but different toroidal rotation velocities are consistent with poloidal rotation driven primarily by neoclassical processes included in NCLASS, including strong poloidal damping.[19] However, large trapped particle orbits are sometimes expected near the axis in ERS plasmas due to low values of B_θ. If the orbit sizes are on the order of or exceed pressure gradient scale lengths, the size ordering usually assumed in neoclassical theory can be violated. An approximate method[22] has been applied to the neoclassical theory described in the NCLASS code to account for reductions in the trapped particle orbit size due to gradients E_r.[23] These calculations indicate that the usual ordering is not violated for r/a of 0.2 or greater in these plasmas, where r is the minor radius and a is the plasma column radius. Inside this radius, this orbit squeezing effect helps preserve the usual ordering. For $r/a < 0.25$, orbit squeezing influences the calculated V_θ through reductions in the effective collisionality as well as a reduction in the diffusive step size of trapped ions, and therefore modifies E_r somewhat (see shaded regions in Fig. 7). This approximate method is used in obtaining all of the results discussed here.

It has been suggested that when the turbulence is deformed by shear flow at a rate comparable to its natural decorrelation rate evaluated in the absence of shear flow effects, transport can be reduced or stopped completely.[24] This is consistent with results from nonlinear simulations[5] of ion-thermal-gradient instabilities. These simulations indicate that a threshold in turbulence-induced transport is realized when $\gamma_{E\times B}/\gamma_{lin}^{max} \sim 1$. When values of this ratio of order unity or above were assumed, turbulence-induced transport ceased. In this work, then, the time behavior of $\gamma_{E\times B}/\gamma_{lin}^{max}$ is used as an indicator of the tendency of shear suppression to be reinforced in a given plasma. Since γ_{lin}^{max} is used as an approximation of the decorrelation rate, which is more difficult to evaluate, the precise value of the ratio of $\gamma_{E\times B}/\gamma_{lin}^{max}$ inferred at the onset of shear suppression should be viewed with caution. In addition, the definition of the shearing rate used here assumes turbulence isotropy, the degree of which may change from condition to condition, and radial and perpendicular decorrelation rates may vary. Differences in the ratio of $\gamma_{E\times B}/\gamma_{lin}^{max}$ at the onset of shear suppression of greater than a factor of two were in fact found in the simulations of Ref. 5, depending on conditions of the baseline plasma, and are also be suggested in recent ERS experiments in which the toroidal field was varied (Section VII).

IV. Bifurcations and possible transition mechanisms

A. The two possible states of reverse-shear plasmas

Proposed transition mechanisms ultimately have to be consistent with the following experimental observations. First, confinement does not degrade, and even improves, as a function of increased pressure gradients. If anomalous transport is driven by fluctuations, any increase of turbulence suppression with pressure gradients must therefore outpace increases in instability drives. Moreover, nearly identical pre-transition conditions can lead to core plasma confinement properties that are strikingly different. This bifurcating quality and sensitivity to initial conditions is highlighted by examining the evolution of two reverse-shear plasmas (Fig. 1). Both have nearly identical heating powers, q profiles, and background plasma parameters in the early state of the plasma evolution. At 2.6 s, however, one of the plasmas had a transition to ERS confinement. Radial profiles of the electron density and pressure are shown in Fig. 2 for a time near the end of the high power heating phase. The large differences in peaking of both quantities highlights the different core confinement properties of these plasmas. For the purposes of this study, analysis is concentrated near r/a = 0.25 - 0.3. This radius is typically in the outer portion of the high confinement region, and inside the minimum in the q profile.[1,4] It also is a region of steep gradients of plasma profiles, allowing for the most reliable inferences of theoretical and experimental quantities.

B. E×B shear flow, Δ'-induced stabilization, and a proposed combined transition picture

The suggestion[11] that E_r is key in balanced-injection TFTR ERS plasmas takes the following form: central fueling and heating results in steep gradients in the plasma pressure, which yield large gradients in E_r and the E×B flow shear. With sufficiently large flow shear, turbulence levels are suppressed and a reduction in transport results. If the pressure gradient is sufficiently large, increases in turbulence suppression with increased ∇p outpace increases in instability growth rates that would occur in the absence of E×B shear. This condition thus leads to a further increases in ∇p and confinement. In this picture, the large Shafranov shifts in these low core-current-density plasmas provide a secondary, but important, influence. These shifts lead to increased ∇p and E×B shear on the outer midplane as compared to plasmas of similar stored energies but peaked current densities. An analogous picture of this positive feedback mechanism that is based on improved momentum confinement can be made for plasmas whose electric field is determined predominantly by rotation.

The alternative viewpoint for the formation of core transport barriers relies on the role of the Shafranov shift Δ itself, or more properly its gradient Δ'. Reduction of instability drives and the formation and sustainment of transport barriers is predicted to occur for some TFTR reversed shear plasmas as a result of favorable precession of barely trapped particles induced by large gradients in the Shafranov shift Δ'.[13] Large Δ' leads to reduced instability drive of trapped electron modes and to reductions in growth rates and fluxes. For significantly large Δ', increasing the magnitude of ∇p leads to a dramatic drop in predicted particle and energy fluxes that is reinforced as more auxiliary heating is applied. Similar arguments were made examining ballooning-type instabilities in the plasma edge.[14]

Both views suggest a combined picture in which large values of Δ', while perhaps not leading to a bifurcation on its own, yields a growth rate reduction that enables the E×B shear to be effective in suppressing turbulence. The presence of both effects reduces the requirements of either to be completely effective on its own while still initiating a bifurcation. Elements of this combined view are suggested in Figure 3. There, the time evolution of $n_e(0)$ for an ERS plasma is shown. Also shown is the E×B shearing rate, $\gamma_{E\times B}$, inferred from the carbon force balance equation, and γ_{lin}^{max}, the linear growth rate of the fastest growing mode. The radius of the calculated and inferred rates corresponds to the outer portion of the region in which fluctuation levels become low in the ERS phase,[4] and confinement is high. At the start of high power neutral beam injection, $\gamma_{E\times B}$ rises with increasing ∇p. Simultaneously, γ_{lin}^{max} changes only slowly as ∇p increases, as a result of turbulence suppression from Δ'-induced effects. After the onset of enhanced confinement with balanced injection, ∇p and $\gamma_{E\times B}$ continue to increase, while γ_{lin}^{max} does not change significantly in this case. This drives $\gamma_{E\times B}/\gamma_{lin}^{max}$ to larger and larger values, suggesting that shear suppression of turbulence is being reinforced. Significantly, gyrofluid calculations indicate that if Δ' stabilization effects are ignored, then the linear growth rate continues to increase with ∇p, much like $\gamma_{E\times B}$. Thus, theory suggests that the presence of Δ' effects eases the requirements for obtaining increasing E×B shear stabilization with positive feedback as the pressure gradient increases. However, it is not ruled out that positive feedback in the absence of Δ' effects could exist.

Just as turbulence suppression is indicated in the discussion above, turbulent fluctuation levels in the core decrease at the ERS transition time. Shown in Fig. 4 are fluctuation levels for two reverse-shear plasmas, one with an ERS transition (29 MW total power injected), the other without (27 MW). For these plasmas, the high power period of injection started at 2.5 s. The fluctuation levels were measured near the radius that eventually forms the boundary of the high confinement region of the ERS case.[4] Also shown are $\gamma_{E\times B}$ and γ_{lin}^{max} for an ERS and RS plasma during this time period. In both plasmas, early times are characterized by bursting fluctuations, measured by reflectometry,[4] that are reminiscent of ELMing behavior at the periphery of H-mode plasmas, and suggesting a competition between instability drive and suppression phenomena. In the ERS plasma, however, these core fluctuation levels fall abruptly at the transition time. In addition to the threshold character, positive feedback is suggested again, as $\gamma_{E\times B}/\gamma_{lin}^{max}$ increases after the transition. In the plasma without the ERS transition, bursting fluctuations at this radius persist past the ERS transition time. Although the behavior of γ_{lin}^{max} early in time is similar to that seen in the ERS case, the shearing rate is smaller early in time for the RS plasma. At that time, the RS plasma pressure is slightly lower, but more importantly this plasma had less counter-injected neutral beam power than the ERS plasma. In general, the $V_\phi B_\theta$ term subtracts from the ∇p_C and the $V_\theta B_\phi$ terms in the carbon force balance equation for these plasmas. Thus, increasing V_ϕ in the co-injection direction leads to a reduction in E_r and its gradient, and smaller values of $\gamma_{E\times B}$ in the RS plasma as compared to the ERS case**.** In the RS case, these shearing and growth rates assume a steady-state behavior after 2.7 s. In the context of this model, this indicates that a critical threshold for shear suppression may have been approached but was never met, and the turbulent state persisted.

It is instructive to point out the role of reversed magnetic shear in this combined picture. Magnetic shear reversal may contribute to transport barrier formation in at least four ways.

1. For a given plasma stored energy, a plasma with a hollow core current density profile as compared to one with a peaked current density profile will yield larger Shafranov shift gradients.

This leads to both a reduction in expected growth rates and fluxes, and a weakened or inverse dependence of the growth rates on the pressure gradient.

2. Compared to plasmas with peaked current density profiles with balanced injection, the larger Shafranov shifts that result from hollow current profiles yield larger values of ∇p on the outer midplane and larger values of E_r and its gradient, leading to increased values of $\gamma_{E\times B}$ (eqs. 2 and 3).

3. Large values of the inverse scale length of B_θ that result from a hollow current profile can also lead to an increase in $\gamma_{E\times B}$, depending the shape of B_θ relative to the local radial electric field (eq. 2).

4. For given pressure and velocity profiles, theory predicts a reduction, typically 25 - 50%, in the calculated instability growth rates as a result of reversed magnetic shear itself.

Item (1) is discussed above, and (2) and (3) are discussed in more detail below. While these effects may make plasmas with shear reversal more conducive to transport barrier formation, it must be emphasized that *shear reversal is not a necessary condition* for such evolution. In fact, spontaneous confinement increases in beam-heated plasmas with monotonic q profiles in supershot-like conditions have been observed on TFTR. The possible roles of E×B shear and Shafranov shift in establishing these conditions is the subject of ongoing study.

V. High power injection at different times in the current evolution

Shown in Figure 5 is a database plot of the power used to obtain ERS transitions in 1.6 MA, 4.6 T reverse shear plasmas as a function of the start time of the high power beams. The high power period followed similar 7 MW heating phases in which the shear reversal was established. Power is not the only factor determining whether or not an ERS transition occurs, but the probability of obtaining an ERS transition does increase with neutral beam injection power at a given time for a given target condition. The likelihood of obtaining an ERS transition at a given power is highest with the earliest injection times. For example, with high power injection at 1.9 s, nearly the full complement of neutral beam injection, about 27 - 30 MW, was required to obtain a transition. However, a reduction in the required power of about 6 MW was achieved by moving this phase of injection earlier.

The changes in power threshold with injection time are consistent with increased contributions from both E×B shear and Δ' effects at the earlier times. The E×B shearing rate falls with later injection as a result of two factors related to the current profile. First, the inverse scale length of the poloidal magnetic field is larger at the radius of peak E×B shearing rate earlier in the current evolution (Fig. 6(a)). Its slow relaxation is qualitatively consistent with the decreasing likelihood of obtaining an ERS transition with late injection. Inside the brackets of eq. 2, $1/B_\theta(dB_\theta/dR)$ dominates over $1/E_r(dE_r/dR)$ near the radius of maximum E×B shear during the early periods of high power neutral beam injection. As a result, the magnetic shear has considerable influence over the magnitude of the total E×B shearing rate. Second, comparatively hollow current profiles yield increases in E_r for a given plasma stored energy as a result of larger Shafranov shifts and pressure gradients on the outer midplane. The importance of E_r itself in determining $\gamma_{E\times B}$ arises through the coefficient in front of the brackets in eq.3. With balanced injection, the pressure gradient usually dominates in the determination of E_r before the onset of enhanced confinement. Shown in Fig. 6(b) is $\nabla p/n$ for carbon for two plasmas. The start of high power injection time was 1.4 and 1.9 s for the two cases, and the two reverse shear plasmas had the same plasma stored energy at the times these profiles were evaluated. However, the stronger Shafranov shift present with the earlier injection time yielded larger values of $\nabla p/n$. This is suggestive, as this plasma had an ERS transition within 10 ms of the time corresponding to the profile shown, while the plasma with 1.9 s injection had no transition. Finally, the larger Shafranov shifts present with early injection for a given local pressure, temperature, and density have a stabilizing influence of instability growth rates, as described in Section IV. Thus, any E×B shear may be more effective in stabilizing the turbulence for a given stored energy at the earlier injection times.

VI. Back-transitions and separation of Δ' and ExB effects

While the observations presented thus far are consistent with both E×B shear and Shafranov shift playing a role in turbulence suppression, holding one constant while varying the other may allow for the evaluation of the necessity of the varied quantity in suppressing turbulence. In these experiments,[25] ERS plasmas were generated with similar neutral beam powers and heating profiles, which fixed quantities central to Δ'-induced stabilization. However, these plasmas had different applied torques and thus varying degrees of toroidal velocity V_ϕ, resulting in changes in E_r and its shear. Constancy in pressure during the ERS phase allowed separation of the role of E×B and Δ' effects. In the high power heating phase for these experiments, 28 MW of nearly balanced neutral beam injection was applied. It was in this high power period that transitions into the ERS regime were obtained. ERS confinement was sustained for variable periods in the subsequent "postlude" period of lower-power heating. During this experiment, twelve neutral beam sources were used in various combinations, with six neutral beams aimed in the direction parallel to the plasma current (co-injection), and six aimed in the counter-current direction. Both sets of co- and counter-injecting neutral beam sources had about 14 MW each of beam power available for injection. Different combinations of co- and counter-injecting beams were applied during the postlude phase to provide variations in V_ϕ, and thus E_r.

Profiles of E_r and its components from the carbon force balance equation are shown in Fig. 7 for a co-rotating plasma at two times. The first time is shortly after the 28 MW balanced phase, and the second is in the earliest stages of the back-transition. The local electron density and pressure gradients at the latter time have just begun to fall. Again, the toroidal rotation term in the force balance equation opposes the pressure gradient term. The ∇p_C and $V_\theta B_\phi$ contributions to E_r are similar between these two times, but as a result of the increasing V_ϕ, the magnitude of E_r drops by a factor of three at r/a = 0.3. At that location, V_ϕ increased from -0.3×10^5 at 2.3 s to 1.5×10^5 m/s at 2.5 s. The $V_\phi B_\theta$ term shown in Fig. 7 is negative in the outer half of the plasma. This is a result of the measured counter-rotation present there, even with co-dominated injected power. NCLASS calculations indicate that the working ion V_ϕ is also counter-directed in this region.

Analysis indicates that the counter rotation is consistent with the presence of a counter-directed torque, established by a radial current of thermal particles that arises to preserve ambipolarity in response to a ripple loss of about 10% of the beam ions.

The plasma pressure and global energy confinement time remained nearly constant throughout the postlude period so long as the discharges remained in the ERS regime. Eventually, however, some of the plasmas suffered a back-transition to poorer confinement, indicated here by a drop in stored energy inside of r/a = 0.3 (Fig. 8). Counter-dominated, balanced, and slightly co-dominated injection sustained ERS confinement until the end of beam injection, but predominantly co-dominated injection reproducibly triggered a back-transition. Pure co-injection yielded the earliest confinement losses.

In the co-dominated postlude plasmas, the loss of core stored energy occurs at different times but at comparable values of $\gamma_{E\times B}$, indicating that E×B shear is necessary to maintain low transport. For any particular plasma, the causal role of E×B shear is emphasized by the fact that reductions in $\gamma_{E\times B}$ precede back-transitions, while all other plasma quantities, including Δ', are constant or nearly constant in time. Also, for similar pressure profiles, the back-transitions occur at different times by at similar values of E_r and its gradient. The fact that core confinement is unchanged above a threshold value of $\gamma_{E\times B}$ is of primary importance. Increases in core local fluctuation levels, measured from reflectometry, are correlated with increases in local transport coefficients in plasmas with back-transitions (Fig. 9). In addition, transport coefficients and fluctuation levels remain low until $\gamma_{E\times B}$ falls below the local value of γ_{lin}^{max}, again suggesting that the linear growth rate may serve as a rough measure of the turbulence decorrelation rate for these plasmas.

For the plasma with co-only injection in the postlude, transport coefficients fall after 2.6 s, and fluctuations drop below system saturation levels after 2.6 s. After this time, the $\gamma_{E\times B}$ profile becomes dominated by gradients in V_ϕ rather than ∇p, suggesting that E×B shear from rotation drive may be reducing turbulence, as has been suggested for DIII-D NCS and VH-mode plasmas.[26] In addition, in all of the plasmas studied, kinetic calculations[27] indicate that the velocity shears in these plasmas are far below those required to excite instabilities[28,29] which might cause a loss in confinement.

VII. B field and rotation scans

Reverse-shear plasmas were generated that take advantage of TFTR's capability to operate over a wide range of toroidal fields. In all cases, the start of the high power injection time was 1.7 s. Using balanced injection, the field was varied from 4.6 T to 2.7 T, and the total plasma current was varied to keep the edge q constant. MSE measurements indicate that the q profile shape was similar as well at comparable times between plasma conditions. A strong variation of the ERS threshold with toroidal field was observed, with the lowest thresholds occurring at the smallest values of B_T. Roughly, the observed power threshold scaled as B_T^2.

Since the details of the target density and temperature profiles differed at the various toroidal fields, the origin of the strong scaling is as yet unclear. Nonetheless, this dataset provides a useful testbed of the range of applicability of $\gamma_{\rm lin}^{\rm max}$ as a measure of the turbulence decorrelation rate. In this study, it was found that the inferred and calculated ratios of $\gamma_{E\times B}/\gamma_{\rm lin}^{\rm max}$ at the time of transition varied significantly with toroidal field. At the highest fields (4.6 T), $\gamma_{E\times B} \sim \gamma_{\rm lin}^{\rm max}$ just before the transition, as in the plasmas discussed earlier. However, at the lowest fields (2.7 T), $\gamma_{E\times B}$ is over a factor of two smaller than $\gamma_{\rm lin}^{\rm max}$. Variations in $\gamma_{E\times B}/\gamma_{\rm lin}^{\rm max}$ of this order at the onset of turbulence suppression were observed in the nonlinear simulations of Ref. 5, where it was emphasized that further tests of the parametric dependence of this critical ratio are necessary. Another possibility is that Δ' effects play a more prominent role in the bifurcation process at lower toroidal fields and current, and that the requirement of E×B flow shear suppression is relaxed.

The low power threshold at low B_T permits studies of the dependence of the forward transition power threshold on co- and counter-injection fraction. Initial analysis indicates that the power threshold is higher with strongly unidirectional injection than with balanced injection. With co-injection, this might be understood in terms of the competition between toroidal velocity and pressure gradient drive in determining E_r that was highlighted in the back-transition study and introduced in Section IV. Given that the pre-transition plasmas have peaked pressure profiles, an increase in core confinement might lead to offsetting increases in the rotational drive of E_r. It is possible, then, that while the plasma remains close to realizing shear suppression of turbulence, the necessary components of a positive feedback scenario are missing. The case of higher power thresholds with counter-injection cannot be understood in these terms, however. Since rotational and ∇p drive of E_r have the same sign, it would appear that the elements of a positive feedback picture are in place. Analysis of these experiments is ongoing, including an examination of the role of weaker pressure gradients usually present in plasmas with counter rotation as compared to plasmas with balanced injection or co-injection, as well as the role of rotationally driven instabilities.

VIII. Discussion

From details presented regarding both the forward transitions and the loss of ERS confinement, it is apparent that the processes involved in suppressing turbulence and reducing transport have a threshold character, and that small differences in plasma conditions can lead to radically different plasmas evolutions. The observations are consistent with at least two elements playing a role in achieving and maintaining good confinement in TFTR ERS plasmas. Theoretical indications are that Δ'-induced stabilization effects reduces ∇p-drive of TEM-like instabilities. Combined with pressure-driven $E \times B$ shear, this increases the likelihood of establishing a positive-feedback picture in which turbulence suppression is reinforced. This point of view is consistent with the observed marked decrease in fluctuation levels near $r/a = 0.3$ at the onset of ERS confinement, and qualitatively describes the dependence of the likelihood of obtaining an ERS transition as a function of high power neutral beam injection time. However, this self-consistent picture does not provide for the unique identification of either $E \times B$ shear or Δ' effects as being causal. Experiments with nearly-steady-state ERS plasmas were performed with the aim of performing such an identification. They point out the necessary role of $E \times B$ shear, and indicate that Δ' effects alone are not sufficient to maintain ERS confinement in these plasmas. As of yet, however, an experimental verification of the necessary role of Δ' has not been performed. The causal role of E_r stems most simply from the correlation of back-transition times with reduced gradients in E_r, and from the inference that the changes in E_r precede any loss in confinement.

The forward transition studies performed by varying the toroidal field and the plasma rotation in part suggest limitations of the simple criterion that $\gamma_{E\times B}/\gamma_{lin}^{max} \sim 1$ in order for turbulence suppression to occur. These observations point to the need for study with respect to the identification of the most relevant shear suppression criterion and its underlying dependencies, and highlight the need for calculations of turbulence decorrelation rates in a fully nonlinear framework that includes rotation- and ∇p-drive of E_r explicitly. An additional challenge for nonlinear theory is to successfully account for the two different timescales of turbulence change that are observed. In Fig. 4, the fluctuation levels fall abruptly at the onset of ERS confinement on a timescale that challenges the time resolution of the measurements. Likewise, the forward transition is often observed as a nearly instantaneous change in the rate of rise in the central particle number. Note, however, that after $\gamma_{E\times B}$ falls below a threshold value in the back-transition work (Fig. 9), the return of the highest fluctuation amplitudes continues over time periods of the order of 100 ms or more.

Work not addressed here includes ERS power threshold studies in tritium operation. Operationally, power thresholds are higher with tritium neutral beam injection.[30] This is surprising, since past power threshold scaling studies of H mode transitions with hydrogen and deuterium suggested a favorable dependence with isotopic mass. The results found in TFTR ERS plasmas is being investigated in the context of the turbulence suppression models discussed here.

A study of the role of Ion Bernstein Wave injection in inducing core transport barriers is underway on TFTR. The aim is to investigate controlled formation and relaxation of transport barriers with the combination of IBW and bi-directional neutral beams in both reverse-shear and monotonic q profile operation. With such control, the location of the transport barrier might be optimized to take advantage of enhanced confinement without suffering the consequences of higher disruptivity that sometimes occurs as a result of the highly localized steep pressure profiles. In addition, since pressure gradient scale lengths often scale with device size, power thresholds of ∇ p-drive of E_r shear may not scale reasonably to a reactor-sized tokamak. Rotationally driven shear may be energetically inefficient a large tokamak as well. IBW research is therefore of high practical importance for the development of a smaller, more economically attractive tokamak concept.

The authors wish to express their appreciation for the efforts and dedication of the TFTR staff and engineers, particularly those involved in tokamak and neutral beam operations. Thanks are due to P.H. Diamond (UCSD) for fruitful discussions and suggestions. Thanks also to W. Houlberg (ORNL) for making the NCLASS code available and for useful conversations pertaining to neoclassical theory. The encouragement of R.J. Hawryluk, J. Hosea, D.W. Johnson, K.M. McGuire, and W.M. Tang is appreciated. This work was supported by DoE Contract No. DE-AC02-76-CH-03073.

[1] F. Levinton, M.C. Zarnstorff, S.H. Batha, M. Bell, R.E. Bell, R.V. Budny, C. Bush, Z. Chang, E. Fredrickson, A. Janos, J. Manickam, A. Ramsey, S.A. Sabbagh, G.L. Schmidt, E.J. Synakowski, and G. Taylor, Phys. Rev. Lett. **75**, 4417 (1995).

[2] E.J. Strait, L.L. Lao, M.E. Mauel, B.W. Rice, T.S. Taylor, K.H. Burrell, M.S. Chu, E.A. Lazarus, T.H. Osborne, S.J. Thompson, and A.D. Turnbull, Phys. Rev. Lett. **75**, 4421 (1995).

[3] L. Lao, K.H. Burrell, T.S. Casper, V.S. Chan, M.S. Chu, J.C. DeBoo, E.J. Doyle, R.D. Durst, C.B. Forest, C.M. Greenfield, R.J. Groebner, F.L. Hinton, Y. Kawano, E.A. Lazarus, Y.R. Lin-liu, M.E. Mauel, W.H. Meyer, R.L. Miller, G.A. Navratil, T.H. Osborne, Q. Peng, C.L. Rettig, G. Rewoldt, T.L. Rhodes, B.W. Rice, D.P. Schissell, B.W. Stallard, E.J. Strait, W.M. Tang, T.S. Taylor, A.D. Turnbull, and R.E. Waltz, Phys. Plasmas **3**, 1951 (1996).

[4] E. Mazzucato, S.H. Batha, M. Beer, R.E. Bell, R.V. Budny, C. Bush, T.S. Hahm, G.W. Hammett, F.M. Levinton, R. Nazikian, H. Park, G. Rewoldt, G.L. Schmidt, E.J. Synakowski, W.M. Tang, G. Taylor, and M.C. Zarnstorff, Phys. Rev. Lett. **77**, 3145 (1996)..

[5] R.E. Waltz, G.D. Kerbel, and J. Milovich, Phys. Plasmas **1**, 2229 (1994).

[6] T.S. Hahm and K.H. Burrell, Phys. Plasmas **2**, 1648 (1995).

[7] R. Taylor, M.L. Brown, B.D. Fried, H. Grote, J.R. Liberati, G.J. Morales, P. Pribjl, D. Darrow, M. Ono, Phys. Rev. Lett. **63**, 2365 (1989).

[8] H. Biglari, P.H. Diamond, and P.W. Terry, Phys. Fluids B **2**, 1 (1990).

[9] K. Burrell, E.J. Doyle, P. Gohil, R.J. Groebner, J. Kim, R.J. LaHaye, L.L. Lao, R.A. Moyer, T.H. Osborne, W.A. Peebles, C.L. Rettig, T.H. Rhodes, and D.M. Thomas, Phys. Plasma **1**, 1536 (1994).

[10] K. Burrell, this issue.

[11] P.H. Diamond, V.B. Lebedev, D.E. Newman, B.A. Carreras, T.S. Hahm, W.M. Tang, G. Rewoldt, K. Avinash, "On the Dynamics of Transition to Enhanced Confinement in Reversed Magnetic Shear Discharges," accepted for publication in Phys. Rev. Lett.

[12] M.A. Beer and G.W. Hammett, Bull. Am. Phys. Soc. **40**, 1733 (1995).

[13] M.A. Beer, G.W. Hammett, G. Rewoldt, E.J. Synakowski, M.C. Zarnstorff, and W. Dorland, this issue.

[14] J.F. Drake, Y.T. Lau, P.N. Guzdar, A.B. Hassam, S.V. Novakovski, B. Rogers, and A. Zeiler, Phys. Rev. Lett **77**, 494 (1996)

[15] S. Parker, Phys. Plasmas **3**, part II, 1959 (1996).

[16] M. A. Beer, Ph. D. thesis, Princeton University (1995)

[17] T.S. Hahm and K.H. Burrell, 1996, private communication.

[18] F. Levinton, R.J. Fonck, G.M. Gammel, R. Kaita, H.W. Kugel, E.T. Powell, D.W. Roberts, Phys. Rev. Lett. **63**, 2060 (1989).

[19] M.C. Zarnstorff, F.M. Levinton, S.H. Batha, E.J. Synakowski, Phys. Plasmas, in press.

[20] B.C. Stratton, R.J. Fonck, K.P. Jaehnig, N. Schechtman, E.J. Synakowski, in *Proceedings of the IAEA Technical Committee Meeting on Time Resolved Two- and Three-Dimensional Plasma Diagnostics, Nagoya, Japan* (International Atomic Energy Agency, Vienna, 1991), p. 78.

[21] S.P. Hirshman and D.J. Sigmar, Nucl. Fus. **21**, 1079 (1981).

[22] K.C. Shaing, C.T. Hsu, R.D. Hazeltine, Phys. Plasmas **1**, 3365 (1994).

[23] H.L. Berk and A.A. Galeev, Phys. Fluids **10**, 441 (1967).

[24] H. Biglari, P.H. Diamond, P.W. Terry, Phys. Fluids B **2**, 1 (1990).

[25] E.J. Synakowski, S.H. Batha, M.A. Beer, M.G. Bell, R.E. Bell, R.V. Budny, C.E. Bush, P.C. Efthimion, G.W. Hammett, T.S. Hahm, B. LeBlanc, F. Levinton, E. Mazzucato, H. Park, A.T. Ramsey, G. Rewoldt, S.D. Scott, G. Schmidt, W.M. Tang, G. Taylor, and M.C. Zarnstorff, Phys. Rev. Lett., in press.

[26] R. LaHaye, T.H. Osborne, C.L. Rettig, C.M. Greenfield, A.W. Hyatt, J.T. Scoville, Nucl. Fusion **35**, 988 (1995).

[27] G. Rewoldt, W.M. Tang, and R.J. Hastie, Phys. Fluids **30**, 807 (1987).

[28] N. Mattor and P.H. Diamond, Phys. Fluids. **31**, 1180 (1988)

[29] M. Artun, W.M. Tang, and G. Rewoldt, Phys. Plasmas **2**, 3384 (1995)

[30] S.D. Scott, G.W. Hammett, C.K. Phillips, E.J. Synakowski, S. Batha, M.A. Beer, M.G. Bell, R.E. Bell, R.V. Budny, C.E. Bush, W. Dorland, P.C. Efthimion, D. Ernst, E.D. Fredrickson, J.C. Hosea, S. Kaye, M. Kotschenreuther, F.M. Levinton, Q.P. Liu, R. Majeski, D.M. McCune, D.R. Mikkelsen, S. von Goeler, H.K. Park, A.T. Ramsey, J.H. Rogers, S.A. Sabbagh, G. Schilling, C.H. Skinner, G. Taylor, R. Waltz, J.R. Wilson, M.C. Zarnstorff, Paper IAEA-F1-CN-64/A6-6, to be published in the Proceedings of the Sixteenth International Conference on Plasma Physics and Controlled Nuclear Fusion Research, Montreal, October 1996, International Atomic Energy Agency, Vienna.

Figure captions

Fig. 1. (a). The neutral beam total power waveform for two reverse-shear plasmas. (b). The central electron density for these two cases. The ERS transition is characterized by a strong rise in $n_e(0)$ that begins near 2.6 s. (c). The density peaking factor, ne(0)<ne>. (d). q profiles at the time of transition.

Fig. 2. (a). The electron density profile for the RS and ERS plasmas shown in Fig. 1, 400 ms after the start of the high power phase of injection. (b). The plasma pressure profile at the same time.

Fig. 3. (a) The central electron density $n_e(0)$ for an ERS plasma. (b). Time histories of the shearing rate $\gamma_{E\times B}$ and maximum linear growth rate γ_{lin}^{max} for the ERS plasma at r/a = 0.25. Also shown are calculated values of γ_{lin}^{max} ignoring Δ'-induced stabilization effects.

Fig. 4. (a). $\gamma_{E\times B}$ and γ_{lin}^{max} for an ERS plasma with 29 MW of neutral beam heating. The dashed line represent the time of the ERS transition. (b). Fluctuation levels, measured with reflectometry, near the boundary of the region of good confinement. The clipped signal at the largest fluctuation levels represents saturation of the reflectometer signal. The measurements have an estimated spatial resolution of 1 - 2 cm, and sample a wavenumber range of $0.5 < k < 2.0$ cm^{-1}. (c). Same as (a), but for the RS plasmas. (d). Same as (b), but for the RS case.

Fig. 5 A database plot of the applied heating power vs. time-of-injection for a wide range of reversed shear plasmas with nearly balanced injection. Solid triangles represent discharges with ERS transitions, while open triangle represent reverse-shear plasmas with no transitions. The curved lines bound the power range in which ERS transitions occurred for roughly one-half of the plasmas. For powers above the top curve, ERS transitions were nearly assured. Below the bottom curve, ERS transitions rarely took place.

Fig. 6. (a). The time evolution of $1/B_\theta[\partial B_\theta/\partial R]$ in the outer midplane and in the region of maximum E×B shearing rate in a reverse shear plasma. This term dominates over $1/E_r[\partial E_r/\partial R]$ in Eq. 2. (b). Measured profiles of $\nabla p/n$ for the dominant impurity, carbon, during high power balanced injection. Before high power injection, these plasmas were nearly identical. One had a high power phase that began at 1.4 s, the other at 1.9 s. For both, the balanced injected power was 24 MW, and the plasmas had the same total stored energy at the times these profiles were evaluated.

Fig. 7 Radial profiles of the carbon force balance equation components for one of the co-rotating plasmas during the 14 MW postlude period. For this plasma, $(P_{co}-P_{ctr})/P_{tot} = 0.62$. Components are shown for 2.3 s, 50 ms after the end of the balanced injection period, and at 2.5 s, just at the start of the loss of ERS confinement.. (a). The toroidal rotation term, $V_\phi B_\theta$. (b). The carbon pressure term. (c). The poloidal rotation term, $V_\theta B_\phi$. (d). The sum of the three terms, the radial electric field E_r. The calculations of V_θ include orbit squeezing effects, as described in the text. The shaded region represents the difference in the E_r profile that result if orbit squeezing is ignored.

Fig. 8. (a). The stored energy, integrated out to r/a = 0.3 for plasmas with and without back transitions. This location is near the radius of maximum $\gamma_{E\times B}$ before the back-transition. Curves are labeled according to the difference on co- vs. counter-injected power, P_{co} - P_{ctr}, divided by the total injected power P_{tot}. The vertical bars denote the times the stored energy begins to fall. (b). $\gamma_{E\times B}$ at r/a = 0.3. Also shown (squares) is the linear growth rate γ_{lin}^{max} for the co-dominated case with the latest back-transition. Growth rates for the other plasmas during their 14 MW postlude ERS phases are comparable. (c) The gradient in the Shafranov shift, Δ', at r/a= 0.3.

Fig. 9 The effective particle diffusivity D_{eff}, and measured fluctuation amplitudes at r/a = 0.3 for plasmas with (a) all co-injection (b) balanced injection in the postlude.

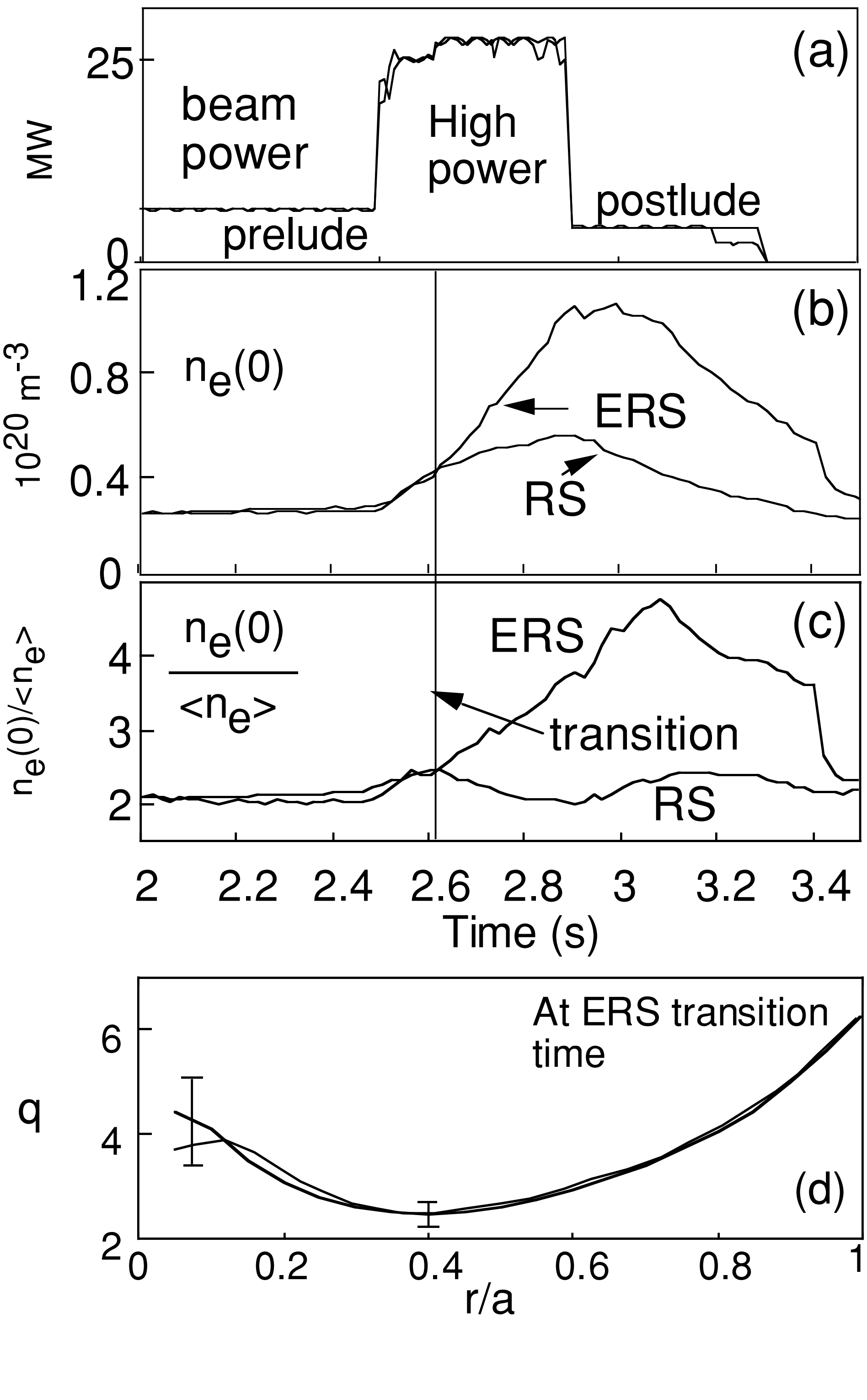

(a)
25
0
MW
beam
power
prelude
High
power
postlude
(b)
1.2
0.8
0.4
0
10^{20} m^{-3}
$n_e(0)$
ERS
RS
(c)
4
3
2
$n_e(0)/\langle n_e\rangle$
$\frac{n_e(0)}{\langle n_e\rangle}$
ERS
transition
RS
2
2.2
2.4
2.6
2.8
3
3.2
3.4
Time (s)
At ERS transition
time
6
4
2
q
(d)
0
0.2
0.4
0.6
0.8
1
r/a

Figure 1

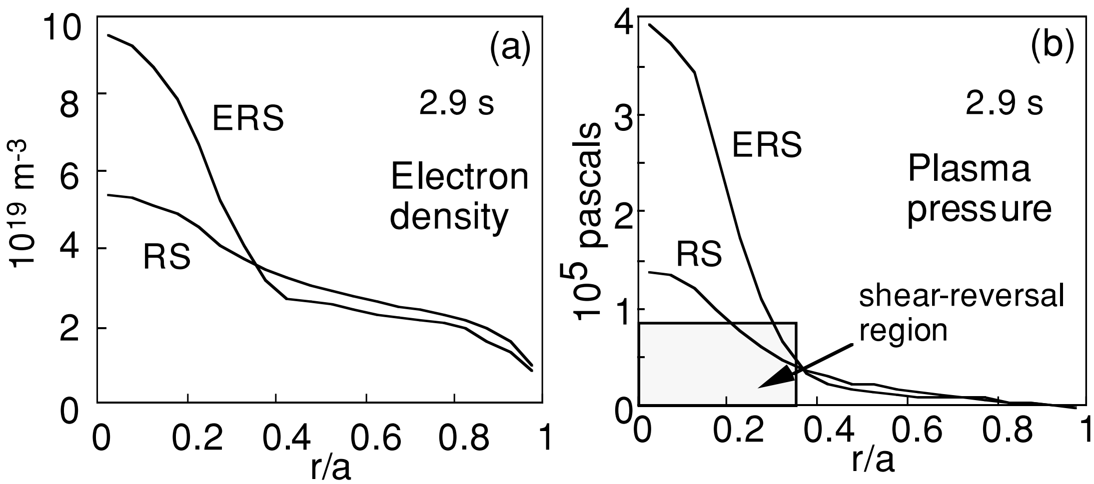

(a)
2.9 s
ERS
RS
Electron density
10^{19} m-3
r/a
(b)
2.9 s
ERS
RS
Plasma pressure
10^5 pascals
shear-reversal region
r/a

Figure 2

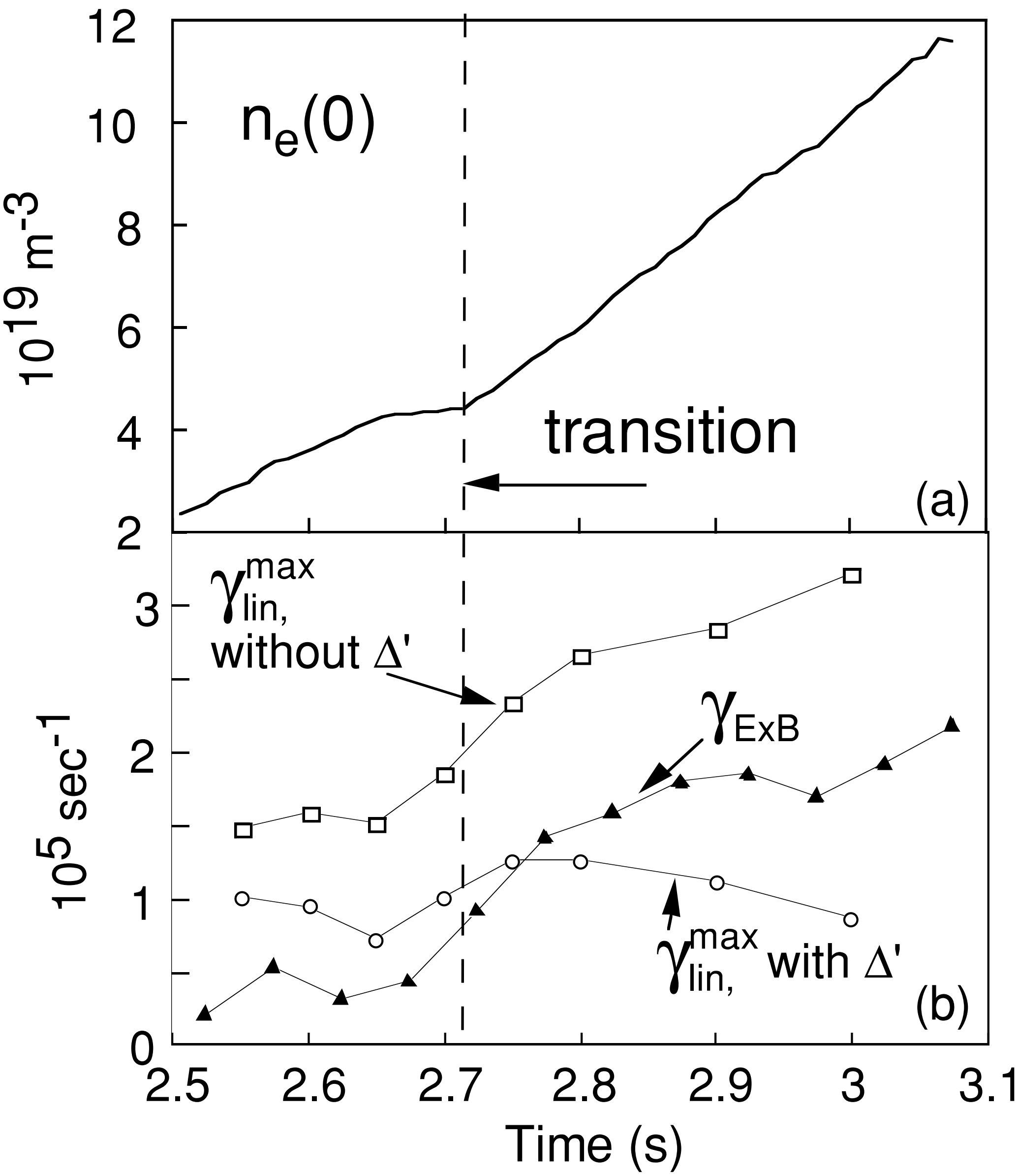

$n_e(0)$
$10^{19}\,m^{-3}$
transition
(a)
$\gamma^{max}_{lin,}$ without Δ'
γ_{ExB}
$\gamma^{max}_{lin,}$ with Δ'
(b)
$10^5\,sec^{-1}$
Time (s)

Figure 3

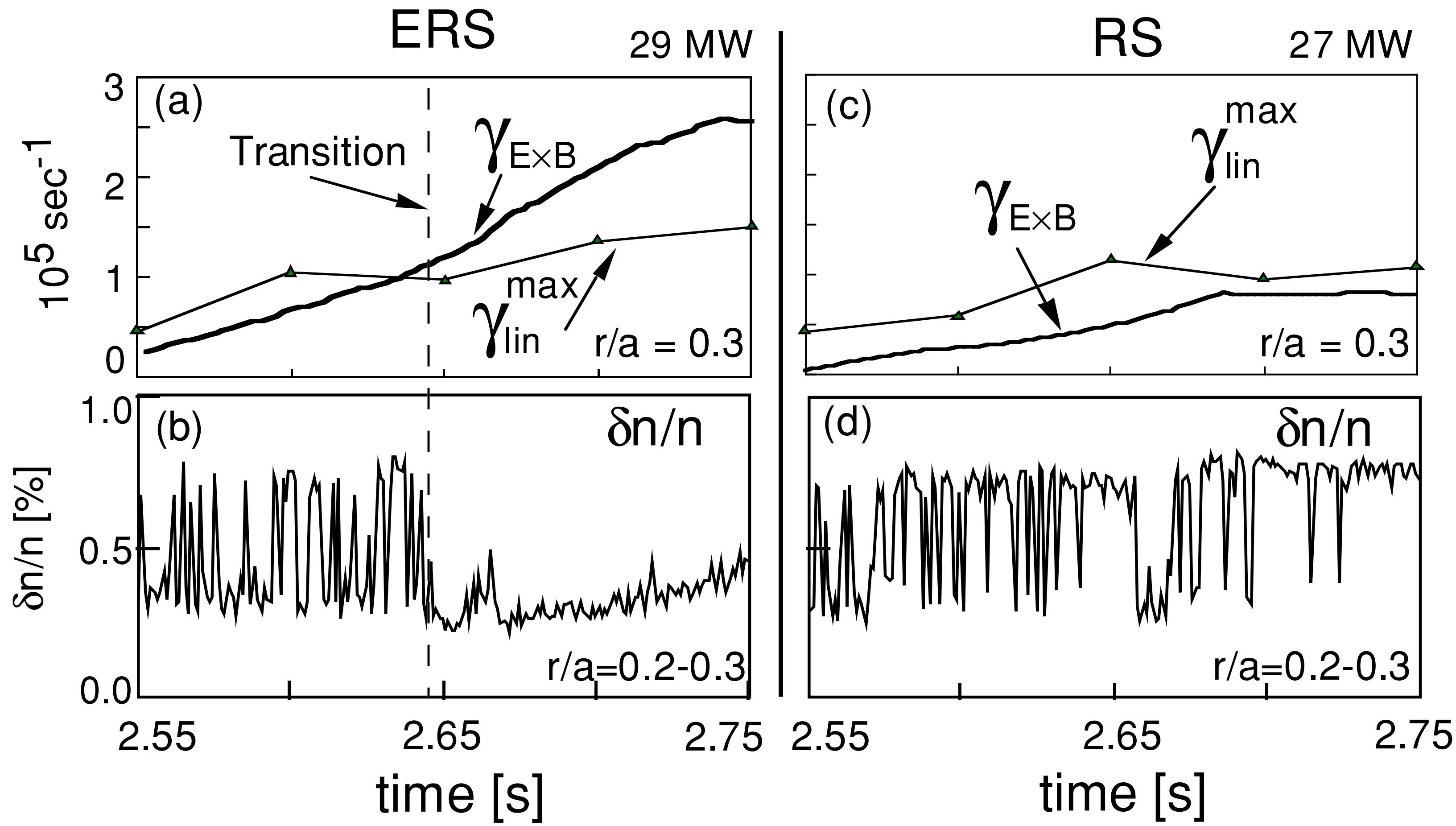

ERS
29 MW
RS
27 MW
(a)
(b)
(c)
(d)
Transition
$\gamma_{E\times B}$
γ_{lin}^{max}
r/a = 0.3
δn/n
r/a=0.2-0.3
10^5 sec^{-1}
δn/n [%]
3
2
1
0
1.0
0.5
0.0
2.55
2.65
2.75
time [s]

Figure 4

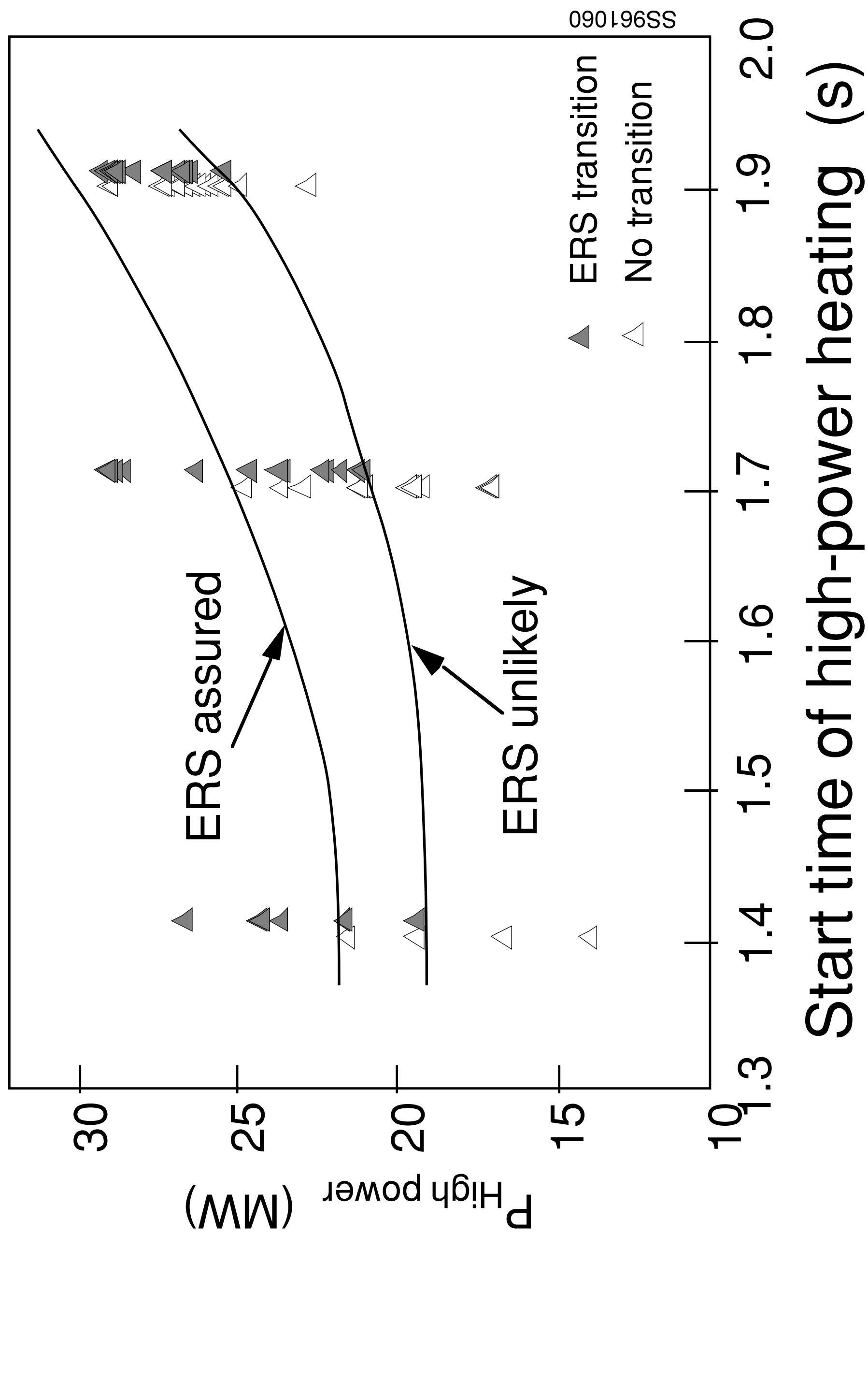

ERS assured
ERS unlikely
ERS transition
No transition
SS961060
Start time of high-power heating (s)
P High power (MW)
1.3
1.4
1.5
1.6
1.7
1.8
1.9
2.0
10
15
20
25
30

Figure 5

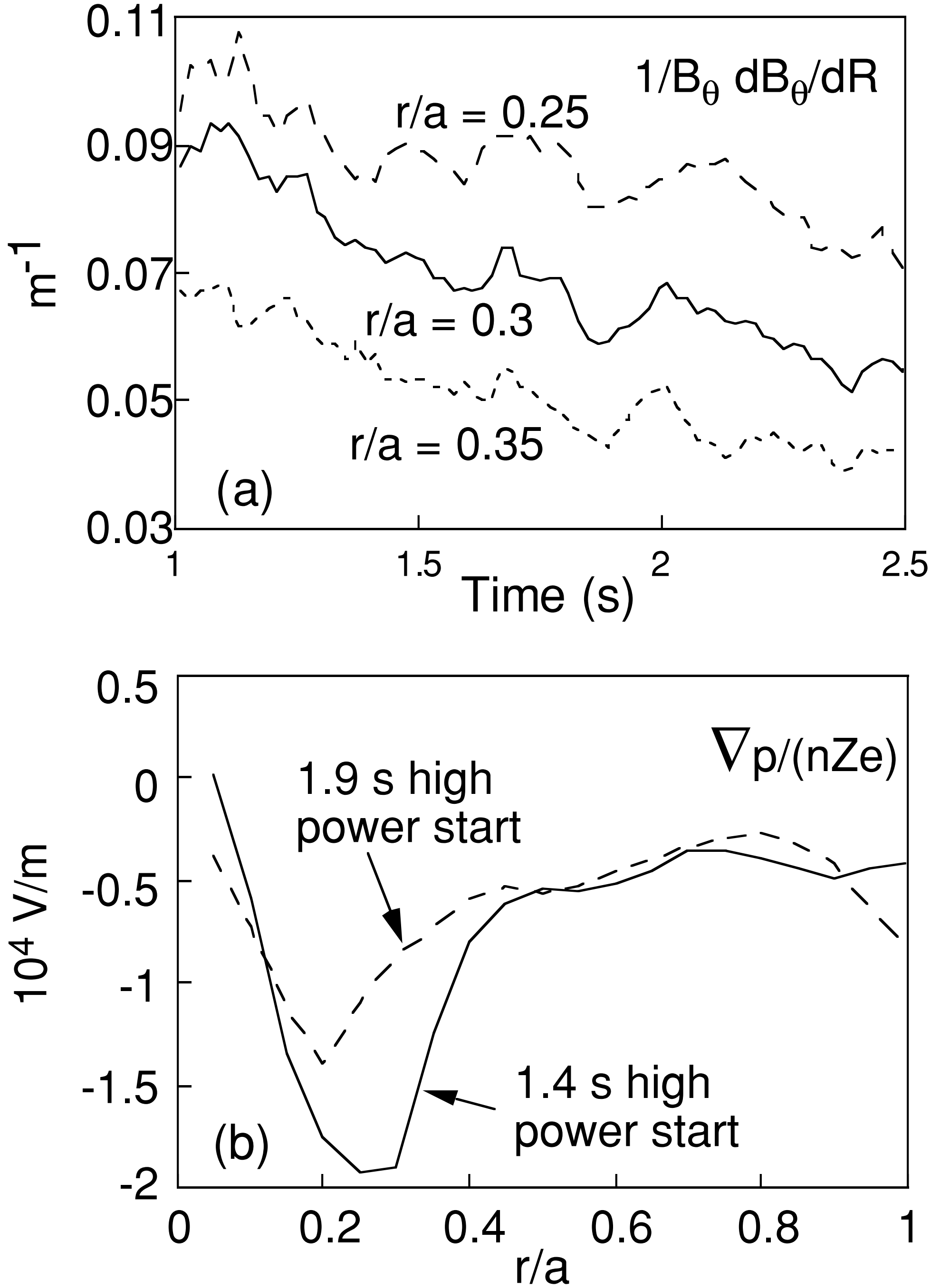

0.11
0.09
0.07
0.05
0.03
m-1
1/Bθ dBθ/dR
r/a = 0.25
r/a = 0.3
r/a = 0.35
(a)
1
1.5
2
2.5
Time (s)
0.5
0
-0.5
-1
-1.5
-2
10⁴ V/m
∇p/(nZe)
1.9 s high
power start
1.4 s high
power start
(b)
0
0.2
0.4
0.6
0.8
1
r/a

Figure 6

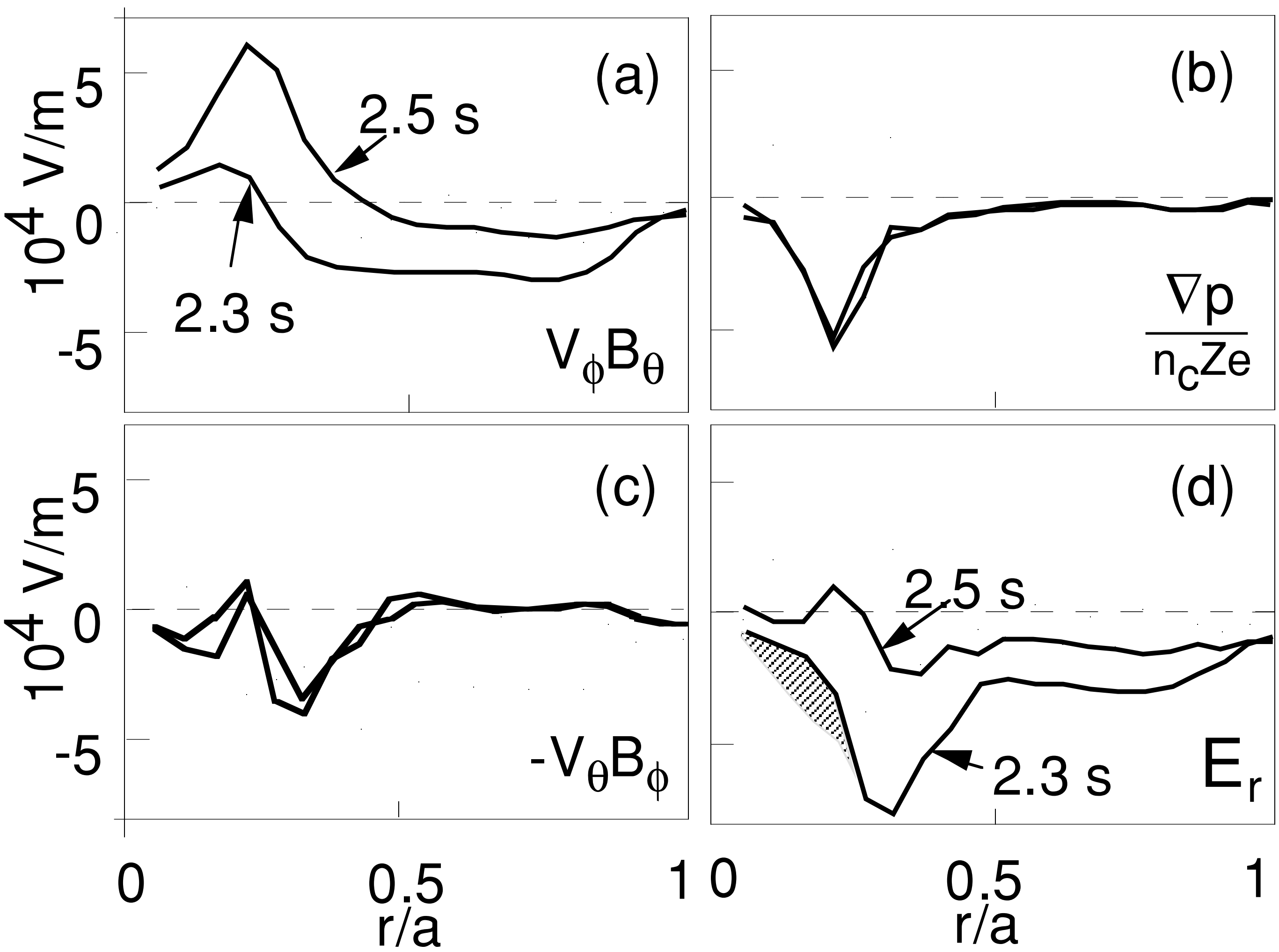
(a)
2.5 s
2.3 s
$V_\phi B_\theta$
(b)
$\frac{\nabla p}{n_c Z e}$
(c)
$-V_\theta B_\phi$
(d)
2.5 s
2.3 s
E_r
10^4 V/m
5
0
-5
0
0.5
1
r/a

Figure 7

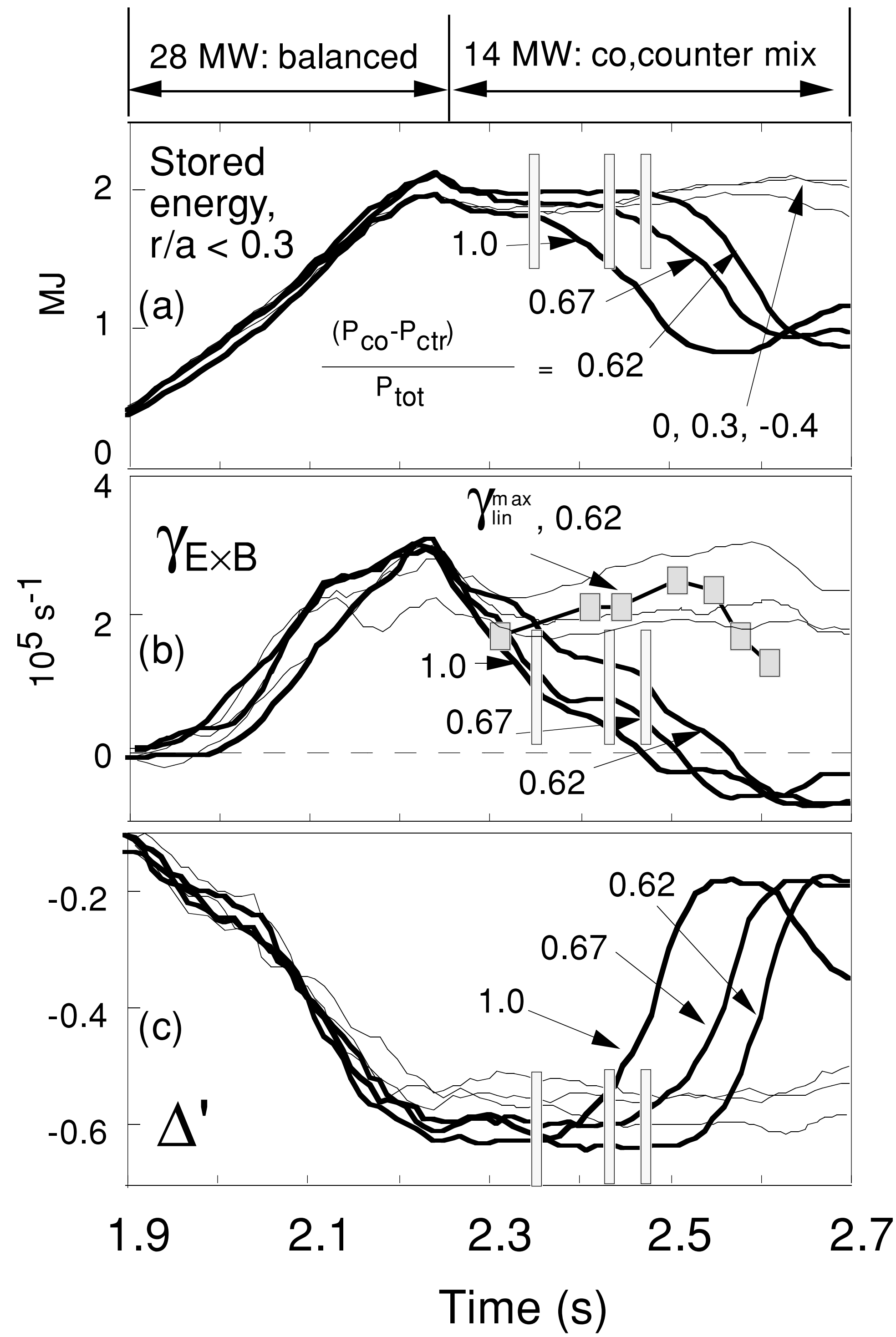

28 MW: balanced
14 MW: co,counter mix
Stored energy, r/a < 0.3
MJ
(a)
1.0
0.67
0.62
0, 0.3, -0.4
(P$_{co}$-P$_{ctr}$) / P$_{tot}$ =
$\gamma_{E\times B}$
γ_{lin}^{max}, 0.62
$10^5\ s^{-1}$
(b)
(c)
Δ'
Time (s)

Figure 8

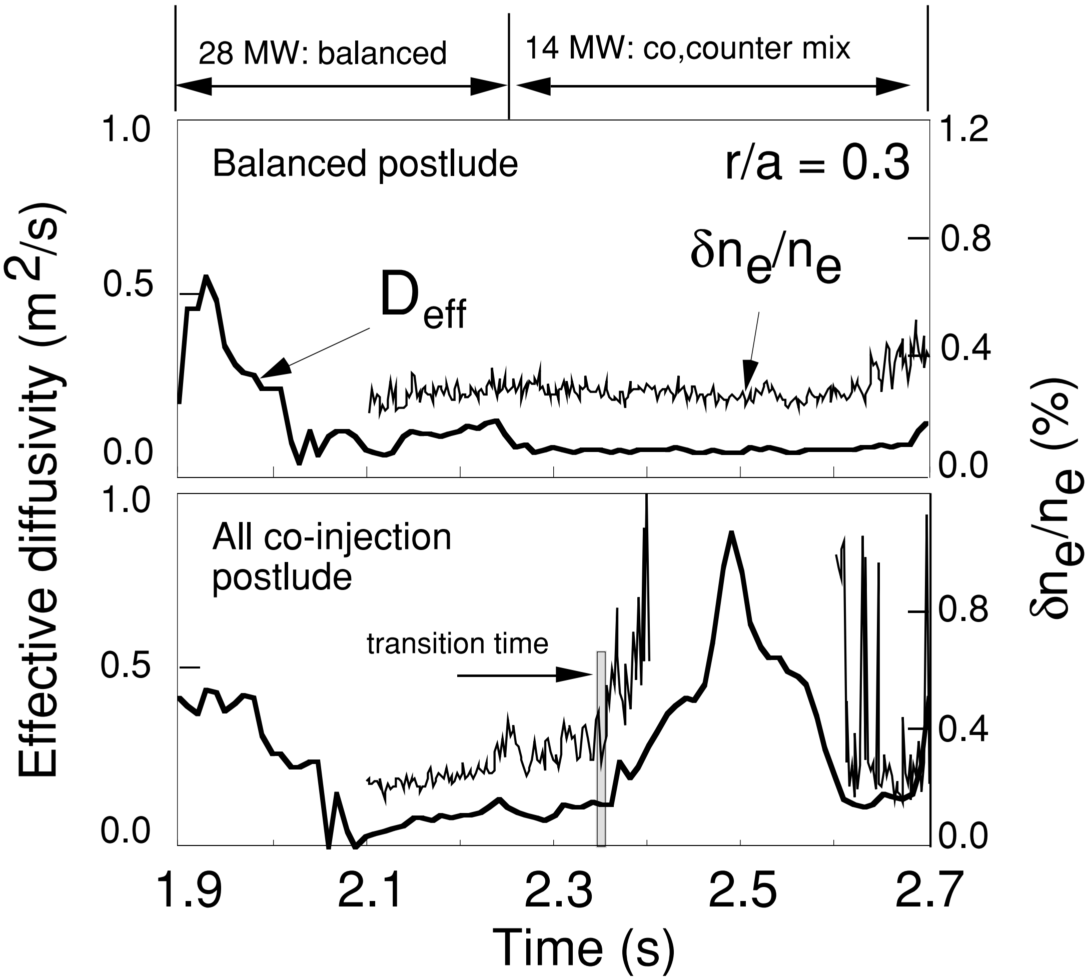

28 MW: balanced
14 MW: co,counter mix
Balanced postlude
r/a = 0.3
D_eff
δn_e/n_e
All co-injection postlude
transition time
Effective diffusivity (m^2/s)
δn_e/n_e (%)
1.0
0.5
0.0
1.2
0.8
0.4
1.9
2.1
2.3
2.5
2.7
Time (s)

Figure 9